Homogeneous nucleation of water between 200 and 240 K: New wave tube data and estimation of the Tolman length

Homogeneous nucleation of water between 200 and 240 K: New wave tube data and estimation of the Tolman length

V. Holten,[a] D. G. Labetski, and M. E. H. van Dongen
Eindhoven University of Technology, Department of Applied Physics, P.O. Box 513, 5600 MB Eindhoven, The Netherlands

(Received 6 June 2005; accepted 14 July 2005; published online 12 September 2005)

We have measured homogeneous nucleation rates of water at 200–240 K in the carrier gas helium, in the range of $10^{13}-10^{17}$ m^{-3} s^{-1} using an expansion wave tube. The rates agree well with the results of Wölk and Strey [J. Phys. Chem. B **105**, 11683 (2001)] in the range of overlap (220–240 K), and are summarized by the empirical fit $J=S\exp[4.6+0.244T-(906.8-2.914T)/(\ln S)^2]$, with J the nucleation rate in m^{-3} s^{-1}, S the supersaturation, and T the temperature in K. We find that the supersaturation dependence of both our rates and those of Wölk and Strey is lower than classical theory predicts, and that the critical cluster is smaller than the classical critical size. These deviations are explained in the framework of the Tolman theory for surface tension, and the "Tolman length" is estimated from our experimental results. We find a positive Tolman length that increases with decreasing temperature, from about 0.1 Å at 260 K to (0.6±0.4) Å at 200 K. We present a nucleation rate expression that takes the Tolman length into account and show that both the supersaturation and temperature dependence are improved, compared to the classical theory.
 [DOI: 10.1063/1.2018638]

I. INTRODUCTION

Vapor-liquid nucleation of water plays an important role in our environment and numerous industrial processes. It is the first step in the phase transformation of the only substance that occurs naturally in liquid, solid, and vapor forms. In 1897, Wilson[1] studied the onset of nucleation by measuring the critical supersaturation; for about 30 years, researchers have also been able to determine the rate of the homogeneous nucleation of water—an overview of experiments is given in Ref. 2. A recent example of accurate rate measurements are the experiments by Wölk and Strey,[3] performed between 220 and 260 K in a nucleation pulse chamber.

In 2002, Peeters *et al.* published nucleation rates[4] obtained in a pulse-expansion wave tube, down to 200 K. A striking feature of these data was a jump in nucleation rates at 207 K, which was interpreted as a transition from vapor-liquid to vapor-solid nucleation. To confirm this transition, we repeated Peeters's measurements in 2003; these new measurements in the range of 200–240 K and some experimental improvements are presented in this paper. Our new data did not show any transition, so we reanalyzed the results of Peeters *et al.* It was found that an inaccuracy in vapor fraction calculations had caused the apparent jump; the corrected data (published separately[5]) show no evidence of a transition in the nucleation process. Our experimental nucleation rates are summarized by an empirical fit, which we will compare with Wölk and Strey's data in the range of overlap, 220–240 K.

It is usually assumed that the supersaturation dependence of the nucleation rate is accurately predicted by classical nucleation theory (CNT). Equivalently, it is assumed that CNT correctly predicts the number of molecules in the critical cluster. We show that these assumptions do not hold for our experiments and those of Wölk and Strey. The deviations from the classical predictions will be explained with Tolman's surface-tension theory, which is briefly described. At the end of the article, we will estimate from our experiments the "Tolman length," a parameter that describes the dependence of the surface tension on droplet size.

II. CLASSICAL NUCLEATION THEORY

Although a complete expression of the nucleation rate was presented as early as 1935 by Becker and Döring,[6] developments are still ongoing. Some recent improvements have focused on properly accounting for translation of the drop,[7] the influence of the spinodal,[8,9] and cluster size fluctuations.[10] To analyze experiments we will use the nucleation rate expression from CNT, because it is still the most widely used theory. The classical rate J_{cl} is given by

$$J_{cl} = K\exp(-W^*_{cl}/kT). \tag{1}$$

Here k is the Boltzmann constant, T is the absolute temperature, and W^*_{cl} is the work of formation of a critical cluster: a cluster that is in unstable equilibrium with the surrounding vapor. The classical value of the formation work is

$$W^*_{cl} = \frac{16\pi\sigma^3_\infty v_l^2}{3(kT\ln S)^2}, \tag{2}$$

with σ_∞ the surface tension of the planar liquid-vapor interface, v_l the molecular volume, and S the supersaturation. For vapor-carrier gas mixtures at near-atmospheric pressure, the supersaturation can be expressed as

[a]Electronic mail: v.holten@tue.nl

$$S = p_v/p_e = yp/p_e, \tag{3}$$

with p_v the vapor pressure, p_e the equilibrium vapor pressure, p the total pressure, and y the molar vapor fraction.

The factor K in Eq. (1) is the kinetic prefactor, given by

$$K = \sqrt{\frac{2\sigma_\infty}{\pi m_1}} v_1 S \left(\frac{p_e}{kT}\right)^2, \tag{4}$$

where m_1 is the mass of a molecule. This expression for K contains a factor S instead of the S^2 in the CNT result. We will use this modification (known as the $1/S$ correction factor) because it makes the equilibrium cluster size distribution satisfy the law of mass action,[11] although it is not the only correction that does so.[12]

In CNT, the number of molecules n_{cl}^* in the critical cluster is given by the so-called Gibbs-Thomson equation

$$n_{\mathrm{cl}}^* = \frac{32\pi\sigma_\infty^3 v_1^2}{3(kT \ln S)^3}. \tag{5}$$

If we assume that the cluster is a sphere with radius R_{cl}^* and that each molecule occupies a volume equal to the molecular volume, so that the total cluster volume is $(4\pi/3)(R_{\mathrm{cl}}^*)^3 = n_{\mathrm{cl}}^* v_1$, we find for the critical radius

$$R_{\mathrm{cl}}^* = \frac{2v_1\sigma_\infty}{kT \ln S}. \tag{6}$$

A further important relation in nucleation research is the "nucleation theorem" developed by Kashchiev[13,14] and recently generalized by Bowles *et al.*[15] It relates the experimentally measurable $J(S)$ dependence at constant temperature to the molecular composition of the critical cluster. Applied to one-component nucleation of a condensed phase in a dilute vapor, the nucleation theorem reads[14]

$$n^* = \left(\frac{\partial \ln J}{\partial \ln S}\right)_T - 1, \tag{7}$$

with n^* the actual number of molecules in the critical cluster.

III. TOLMAN'S THEORY

In reality, a droplet is a heterogeneity which is characterized by a gradually changing density. In the thermodynamics of Gibbs, this density fluctuation is replaced by a simpler two-phase system: a hypothetical system that consists of a homogeneous spherical droplet embedded in a homogeneous vapor. The pressure of the hypothetical vapor p_{vap} is simply taken equal to the pressure in the real system far away from the droplet. On the other hand, the pressure inside the imaginary droplet p_{liq} is not the pressure in the center of the real density fluctuation, but the pressure of a hypothetical bulk liquid at the same chemical potential as the uniform-density vapor. This equality of chemical potentials implies that we restrict our analysis to *critical* droplets.

The infinitely thin interface between the cluster and the vapor is called the "dividing surface;" its position can be freely chosen. For any dividing surface, the work of formation is given by the exact expression[8]

$$W^* = 4\pi(R^*)^2\sigma(R^*) - (4\pi/3)(R^*)^3\Delta p, \tag{8}$$

where R^* is the radius of the droplet (the location of the dividing surface) and $\Delta p = p_{\mathrm{liq}} - p_{\mathrm{vap}}$. Because W^* and Δp are well-defined physical quantities that do not depend on the choice of a dividing surface, we see that the surface tension σ must depend on this choice. [Once R^* is chosen, Eq. (8) can be seen as a definition of σ.] A commonly used dividing surface is the "surface of tension" (indicated by a subscript s), for which the so-called Laplace equation is valid in its simplest form:

$$R_s^* = 2\sigma_s(R_s^*)/\Delta p, \tag{9}$$

where σ_s is the surface tension at the surface of tension. Another choice is the "equimolar dividing surface" (indicated by subscript e), with a radius R_e^* that is chosen such that

$$4\pi\int_0^\infty [\rho(R) - \rho_v]R^2 dR = (\rho_{\mathrm{l}} - \rho_v)\frac{4}{3}\pi(R_e^*)^3, \tag{10}$$

where ρ_{l} and ρ_v are the liquid and vapor densities in the hypothetical system and $\rho(R)$ is the density in the real system.

We now define the "Tolman length" δ as the radial distance between the equimolar dividing surface and the surface of tension:

$$\delta = R_e^* - R_s^*. \tag{11}$$

The value of δ may depend on the droplet size and can be positive or negative. Tolman[16] derived that for relatively large droplets ($R \gg \delta$) and for a δ that is independent of droplet radius, the dependence of surface tension on droplet size is

$$\frac{\sigma_s(R_s^*)}{\sigma_\infty} = \frac{1}{1 + 2\delta/R_s^*}. \tag{12}$$

In the so-called capillarity approximation, the real surface tension is approximated by σ_∞. Eq. (9) then becomes

$$R_{\mathrm{cl}}^* = 2\sigma_\infty/\Delta p, \tag{13}$$

with R_{cl}^* the radius in the capillarity approximation. Taking the ratio of Eqs. (9) and (13) gives

$$\frac{R_s^*}{R_{\mathrm{cl}}^*} = \frac{\sigma_s(R_s^*)}{\sigma_\infty} = \frac{1}{1 + 2\delta/R_s^*}, \tag{14}$$

which can be rewritten into

$$R_s^* = R_{\mathrm{cl}}^* - 2\delta. \tag{15}$$

This result states that the surface of tension is located at a distance of 2δ from the classical radius. From Eqs. (11) and (15) it follows immediately that

$$R_e^* = R_{\mathrm{cl}}^* - \delta, \tag{16}$$

which shows that the equimolar dividing surface lies between the surface of tension and the classical radius at a distance of δ from each.

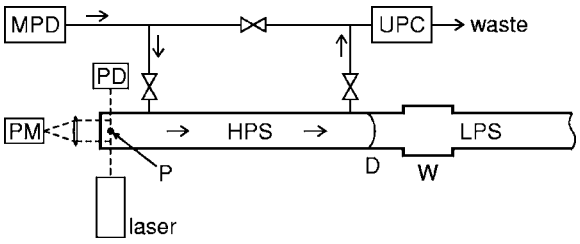

FIG. 1. Schematic top view of the pulse-expansion wave tube setup. MPD: mixture preparation device supplying the $He-H_2O$ mixture, HPS: high-pressure section containing the test mixture, LPS: low-pressure section containing He, *P*: location of pressure transducers, *W*: widening, *D*: diaphragm, UPC: upstream pressure controller, PD: photodiode measuring the transmitted light, PM: photomultiplier measuring the 90° scattered light. The arrows indicate the direction of flushing.

To evaluate the work of formation, we choose the surface of tension as a dividing surface. The Laplace equation, Eq. (9), can then be used to eliminate R^* from Eq. (8), yielding

$$W^* = (16\pi/3)[\sigma_s(R_s^*)]^3/\Delta p^2. \tag{17}$$

In the capillarity approximation, σ_∞ is used instead of σ_s, so that $W_{\mathrm{cl}}^* = (16\pi/3)\sigma_\infty^3/\Delta p^2$. The ratio of the real and classical work of formation is then

$$\frac{W^*}{W_{\mathrm{cl}}^*} = \left[\frac{\sigma_s(R_s^*)}{\sigma_\infty}\right]^3 = \left(\frac{R_s^*}{R_s^* + 2\delta}\right)^3 = \left(1 - \frac{2\delta}{R_{\mathrm{cl}}^*}\right)^3. \tag{18}$$

The second equality follows from Eq. (12) and the last equality from Eq. (15). This result was derived earlier by Abraham[17] and by Schmelzer and Baidakov.[18]

We can now introduce a corrected nucleation rate J_{Tol}, in a form analogous to Eq. (1):

$$J_{\mathrm{Tol}} = K\exp(-W^*/kT) = K\exp[-(W_{\mathrm{cl}}^*/kT)(1 - 2\delta/R_{\mathrm{cl}}^*)^3], \tag{19}$$

where K is the classical prefactor of Eq. (4), W_{cl}^* is given by Eq. (2), and R_{cl}^* is given by Eq. (6). The parameter δ remains unknown at this point and must be estimated by other means. We will describe how to determine it from nucleation rate data in Sec. V F.

IV. EXPERIMENTS

A. Setup

The experiments were performed in a so-called pulse-expansion wave tube,[19,20] which is a modified shock tube (see Fig. 1). The high-pressure section (HPS) serves as a test section in which nucleation occurs. It contains the vapor-carrier gas mixture, which is produced in a dedicated mixture preparation device.[21] We used helium (purity 99.999%) as a carrier gas and varied the molar fraction of water vapor between 2×10^{-4} and 5×10^{-3}, at initial total pressures in the range of 160–270 kPa. The water was purchased from Merck (proanalysi, resistivity >1 MΩ cm). A diaphragm separates the HPS from the low-pressure section (LPS) that contains helium only, at a pressure of about 110 kPa. Before the experiment, the HPS is flushed for 1 h with the test mixture, to ensure adsorption equilibrium with the walls. After the rupture of the diaphragm, the pressure history of Fig. 2 is obtained at the HPS end wall. The pressure dip or pulse, occurring immediately after the large pressure decrease, is caused by pressure waves reflecting from widening *W* in the LPS (Fig. 1) and traveling back into the HPS. The temperature history has a similar shape and is calculated from the pressure using the ideal-gas isentropic relation

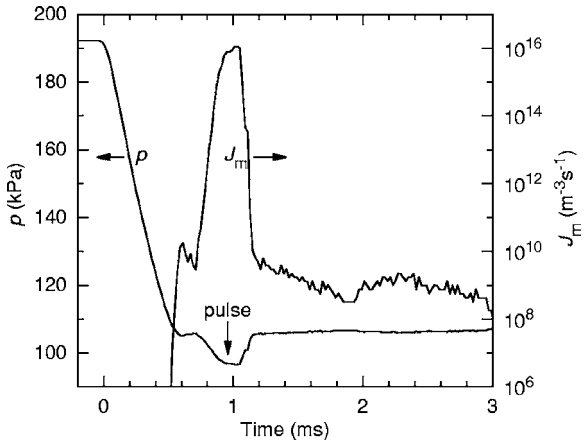

FIG. 2. Typical experimental pressure history at the end wall of the high-pressure section and the theoretical nucleation rate $J_m(t)$ at that position, calculated with Eq. (25). The area under the J_m curve is the predicted droplet number density; in this case $\rho_m = 1.4\times10^{12}$ m^{-3}. The experimental droplet density was $\rho_{\mathrm{exp}} = 3.6\times10^{12}$ m^{-3}. The ratio of these densities is a correction factor for the theoretical nucleation rate in Eq. (24).

$$T = T_0(p/p_0)^{(\gamma-1)/\gamma}, \tag{20}$$

where $\gamma = c_p/c_v$ is the ratio of the specific heats, and p_0 and T_0 are the initial pressure and temperature, respectively. The γ value is corrected for the presence of water vapor in the mixture and lies close to 5/3, the γ of pure helium.

At the beginning of the pulse, the temperature drops by about 10 K. Because the equilibrium vapor pressure p_e depends strongly on temperature, p_e decreases to less than half of its value and consequently the supersaturation S more than doubles. This, in turn, causes the nucleation rate to increase by about six orders of magnitude (see Fig. 2).

At the end of the pulse, the nucleation process is quenched; the amount of droplets formed after the pulse is negligible. The supersaturation remains higher than unity, however, so that the droplets that were formed during the pulse grow to a detectible size. Close to the end wall of the HPS, the number density of droplets ρ_{exp} is determined by a combination of constant-angle Mie scattering at 90° and extinction measurements of a laser beam with a wavelength of 514.2 nm. Finally, the nucleation rate is found as the ratio of the droplet density and the pulse duration Δt:

$$J = \rho_{\mathrm{exp}}/\Delta t. \tag{21}$$

B. Improvements

1. Pressure measurement

The pressure changes at the end wall of the HPS were recorded by a piezoelectric pressure transducer (Kistler type 603B). Transducers of this type measure relative pressure changes, that is, the output voltage difference is proportional

to the pressure difference. Their fast response is a prerequisite for our experiments, but they also have a number of disadvantages. The proportionality constant can only be determined by calibration to a known pressure change, and such a calibration must be done regularly. In addition, the head of the piezoelectric transducer is sensitive to thermal gradients and must be coated; also, the tension which results from mounting influences the characteristics.

To increase the reliability of the pressure measurement, we modified the setup in 2004 to allow an *in situ* calibration of the piezoelectric transducer during the experiment. This was achieved by installing an additional transducer at the end wall, capable of measuring absolute pressures. The new piezoresistive transducer (Kistler type 4043A5) can be calibrated statically (at constant pressure) and is less sensitive to thermal gradients and mounting tension. Although the piezoresistive transducer cannot accurately measure fast pressure changes, it can be used to calibrate the piezoelectric one. The piezoelectric signal is scaled such that it is equal to the piezoresistive signal at a time just before and just after the experiment; in this way the proportionality constant is determined. In our 2004 series of experiments, the maximum deviation of the proportionality constant from the mean was 0.1%, which is within the accuracy of the method of about 0.2%.

2. Pulse conditions

With our setup the droplet density can be determined with a reproducibility better than 5%. However, when calculating the nucleation rate with the traditional method of Eq. (21), this accuracy is lost because the pulse duration is much more uncertain. Ideally, the pulse duration can be defined as the length of the bottom of the pulse where the pressure and temperature are constant. In reality, the edges of the pulse are never sharp and the pressure varies between these edges. The experimenter then has to determine the pulse boundaries by visual inspection of the pressure signal; a subjective method which causes an uncertainty in Δt that can be as large as 30%. In addition, the uncertainty in the position of the pulse edges also introduces errors in the pulse conditions p_{pulse} and T_{pulse}, which are found by averaging over the range between the pulse edges.

To overcome these difficulties, Wölk and Strey[3] fitted the pressure around the pulse with a trapezoidal construction, illustrated earlier by Viisanen *et al.*[22] Our more irregular pulses cannot be easily fitted to such a shape. Instead, we use a method that allows us to obtain the nucleation rate without the subjective definition of the pulse duration: an integration over the entire pressure history. This technique was used by Miller *et al.*[23] and (in a modified form) by Schmitt and co-workers.[24,25] In our case, we integrate a theoretical nucleation rate $J_m(t) \equiv J_m[T(t), S(t)]$ over the entire pressure history, resulting in a modeled droplet density ρ_m:

$$\rho_m = \int J_m(t)dt. \tag{22}$$

Because the value of J_m outside the pulse is orders of magnitude lower than it is during the pulse, ρ_m does not depend on the integration limits as long as the pulse is included in the integration interval. By a similar integration, the pulse conditions p_{pulse} and T_{pulse} can be found. For that purpose we define the pulse pressure as a weighted average over the entire pressure history, where the weight factor is proportional to the number of droplets that were formed at a certain pressure. Using this definition, the weighted pressure average is computed by taking the nucleation rate as a weight factor:

$$p_{\text{pulse}} = \frac{\int p(t)J_m(t)dt}{\int J_m(t)dt} = \frac{1}{\rho_m}\int p(t)J_m(t)dt. \tag{23}$$

The corresponding pulse temperature T_{pulse} is calculated from p_{pulse} by the isentropic relation of Eq. (20). Alternatively, the temperature could be calculated as a weighted average; then $T_{\text{pulse}} = \rho_m^{-1}\int T(t)J_m(t)dt$. In practice, the difference between the two methods is small (1 mK) so either method can be used. The pulse supersaturation S_{pulse} is found from Eq. (3).

To obtain the experimental nucleation rate that corresponds to the pulse parameters T_{pulse} and S_{pulse}, we correct the theoretical nucleation rate with the ratio of experimental and modeled droplet densities,

$$J_{\text{exp}} = \frac{\rho_{\text{exp}}}{\rho_m} \times J_{\text{m}}(T_{\text{pulse}}, S_{\text{pulse}}). \tag{24}$$

The three values T_{pulse}, S_{pulse}, and J_{exp} constitute the result of the integration method and are used in all subsequent graphs and calculations. As mentioned before, the advantage of the integration method is the elimination of subjectiveness; a disadvantage is the need for a nucleation rate model. However, as we will see later, the choice of a particular model has little influence on the results.

C. Accuracy

Nucleation rates are known with about 25% accuracy. The uncertainty in the conditions of the 2003 results is 0.7% in p_{pulse}, 0.5 K in T_{pulse}, and 3%–8% in S_{pulse} (higher uncertainty at low temperature). Because of the new pressure calibration, the conditions of the 2004 results are known with a slightly higher accuracy of 0.4% in p_{pulse}, 0.3 K in T_{pulse}, and 3%–4% in S_{pulse}.

V. RESULTS

A. Experimental supersaturations

Experiments were performed at pulse temperatures between 200 and 240 K at constant nucleation pressures of about 100 kPa. Figure 3 shows the supersaturation during the nucleation pulse, obtained with Eq. (3), for our experiments and those of Wölk and Strey.[3,26] With decreasing temperature, the supersaturation must be increased to keep nucleation rates within the experimental measurement window, in our case 3×10^{13}–3×10^{17} $\text{m}^{-3}\,\text{s}^{-1}$. At equal temperature, the supersaturations of Wölk *et al.* are lower than ours, reflecting the lower nucleation rate window of 10^{11}–10^{15} $\text{m}^{-3}\,\text{s}^{-1}$ of their nucleation pulse chamber. Their

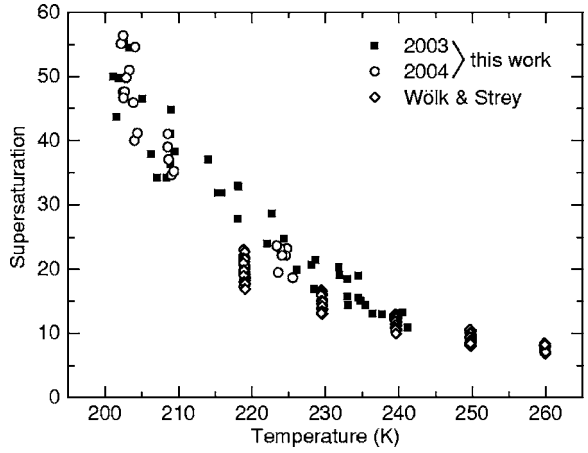

FIG. 3. Supersaturation in the nucleation pulse as a function of the nucleation temperature. Shown are our 2003 and 2004 datasets, and the data of Wölk and Strey (Refs. 3 and 26) obtained in a nucleation pulse chamber.

data consist of five isothermal sets spaced roughly 10 K apart, while our 2003 dataset is more evenly spread across the 200–240 K range. In 2004 we also performed isothermal measurements at 203, 209, and 224 K. Compared to the isotherms of Wölk and Strey, our isotherms have more scatter in the temperature; at most a 1-K deviation from the mean isotherm temperature. These deviations occur because pressure pulses cannot always be accurately reproduced with our setup.

B. Empirical fit of nucleation rates

We proceed now to the way our nucleation rates were obtained. Lacking a nucleation rate model, the first step was to analyze the experiments with the traditional method, by manually defining the pulse duration and using Eq. (21) to obtain J. This procedure yielded a set of preliminary nucleation rates. In order to get a nucleation rate model, the function

$$J_{\mathrm{fit}}(T,S) = J_0 S \exp\left[a_0 + a_1 T - \frac{b_0 + b_1 T}{(\ln S)^2} \right] \tag{25}$$

was then fitted to the preliminary 2003 nucleation rate data, with a_0, a_1, b_0, and b_1 as fitting parameters and $J_0 = 1\ \mathrm{m^{-3}\ s^{-1}}$. This function is based on the empirical formula of Miller *et al.*,[23] but has fewer fitting parameters and a preexponential factor of S instead of S^2. The factor J_0 is included for dimensional consistency. When the logarithm of Eq. (25) is taken, the model becomes linear in the parameters, so that they can be determined by a least-squares linear fitting procedure.

Having available a nucleation rate model, the next step was an analysis using the integration method. The maximum differences of the integration results with the preliminary dataset were 40% in J, 0.3 K in T, and 0.4% in p. The fact that these differences are not too large indicates that the accuracy of the traditional method is acceptable. However, because the pulse integration method eliminates human subjectiveness, it decreases the scatter in the results.

To improve the accuracy even further, Eq. (25) was again fitted to the newly obtained data, after which the pulse integration method was reapplied to update nucleation rates, temperatures, and pressures. This procedure was repeated several times until the fitting parameters changed by less than 0.01%. The results were

$$a_0 = 4.6, \quad a_1 = 0.244\ \mathrm{K^{-1}},$$
$$b_0 = 906.8, \quad b_1 = -2.914\ \mathrm{K^{-1}}, \tag{26}$$

valid for temperatures between 200 and 240 K and nucleation rates in the range of 3×10^{13}–$3\times10^{17}\ \mathrm{m^{-3}\ s^{-1}}$. The fit function J_{fit} reproduces almost all of our 2003 nucleation rates within a factor of 2 (Fig. 4), which is an acceptable error when we take into account the uncertainties of the experimental rates, temperatures, and supersaturations.

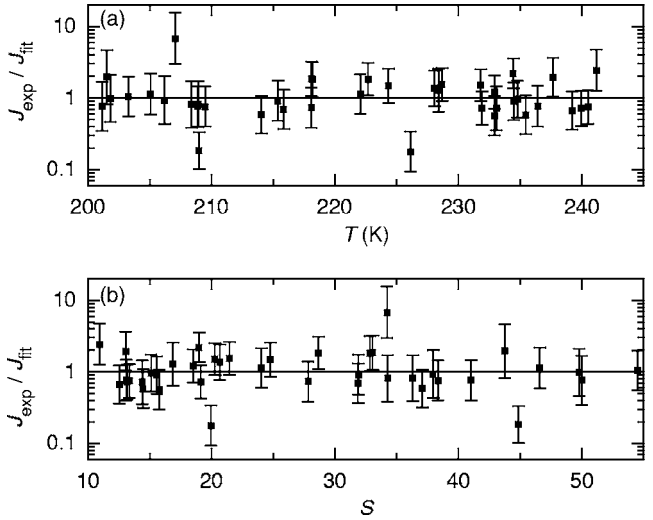

FIG. 4. Ratio of the experimental nucleation rates of 2003 and the J_{fit} function of Eq. (25), (a) as a function of the temperature; (b) as a function of the supersaturation. The residuals show no systematic T or S dependences; therefore Eq. (25) is considered a good fit to the 2003 nucleation data. The error bars combine the uncertainty of J_{exp} (about ±25%) and the uncertainty of J_{fit} (about a factor of 1.8) caused by the errors in T and S.

Finally, to examine the sensitivity of the integration method on the specific model used, we analyzed all experiments using J_{cl} [Eq. (1)] as the model instead of Eq. (25). Although the predictions of J_{cl} differ by several orders of magnitude from J_{fit}, the resulting J_{exp} changes only a few percent. We therefore conclude that the integration method is relatively insensitive to the rate model and the resulting nucleation rates are reliable.

C. Comparison with the Wölk and Strey results

In Fig. 5 the nucleation rates of the three isotherms in our 2004 series and those of three Wölk and Strey isotherms are plotted as a function of the supersaturation. For comparison, the fit of the 2003 rates has been evaluated at the mean temperatures of the six isotherms (dashed lines). The fit agrees well with the Wölk and Strey isotherms, both in value and in slope, and provides a plausible extension of their nucleation rates to lower temperatures and higher supersaturations.

The points of the 2004 isotherms, indicated by open circles, again show the scatter that is partially caused by

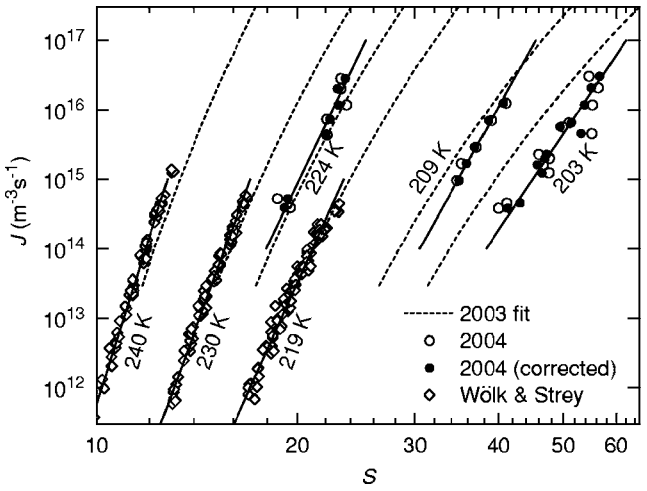

FIG. 5. Nucleation rates as a function of the supersaturation. The open circles show the original 2004 results; the filled circles are the results after the supersaturation is corrected for temperature deviations, as in Eq. (27), which decreases the scatter. The unbroken lines are least-squares straight line fits to the corrected data; their slope decreases at lower temperature. Also shown are three isotherms of Wölk and Strey with least-squares fits. The dashed lines are isotherms of the 2003 fit of Eq. (25) calculated at the mean temperatures of the 2004 isotherms and the Wölk and Strey isotherms.

deviations of the nucleation temperature. It is possible to correct for the scatter in temperatures in a model-independent way, as follows. For each experiment, we estimate the supersaturation S_{corr} that is obtained when the temperature is made equal to the mean isotherm temperature T_{mean}, while keeping the nucleation rate constant. In a first-order approximation, S_{corr} is then

$$S_{\mathrm{corr}} = S + \left(\frac{\partial S}{\partial T}\right)_J (T_{\mathrm{mean}} - T). \tag{27}$$

To use this expression, the derivative $(\partial S/\partial T)_J$ is required. Looijmans and van Dongen[20] and Luijten and van Dongen,[27] who also used Eq. (27), calculated it from CNT. Instead, to analyze our results in a more theory-independent way, we derived it from our experimental data, as follows. First, Eq. (25) was solved for S to obtain S as a function of J and T; then, partial differentiation with respect to T gave the required derivative. The corrected results, indicated by the filled circles in Fig. 5, indeed show that the correction succeeds in reducing the scatter.

D. Comparison with classical nucleation theory

Let us now compare the experimental nucleation rates with the CNT predictions of Eq. (1). This is conveniently done by plotting the ratio of the experimental rates and the CNT rates as a function of temperature, as in Fig. 6(a). Only at 260 K there is agreement between experiment and theory; at lower temperatures the deviation increases—at 200 K the experimental rates are a factor 10^4–10^6 higher than predicted. This deviation, which is caused by the incorrect temperature dependence of the CNT nucleation rate, is well known and observed in almost all water nucleation experiments[2] and also in the nucleation of other substances such as nonane[28] and *n*-alcohols.[29] Apart from the incorrect temperature dependence, the vertical scatter of the scaled

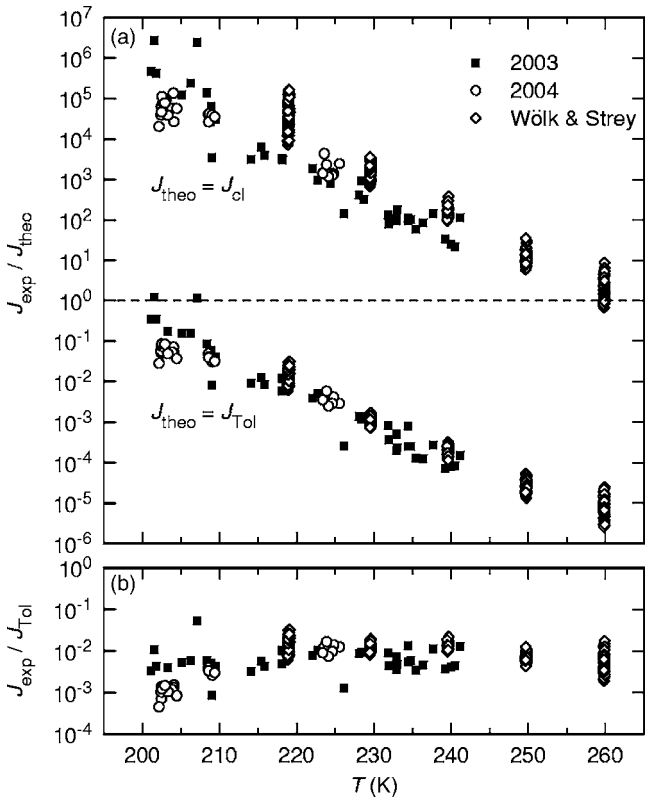

FIG. 6. Ratio of the experimental and theoretical nucleation rates as a function of the temperature, for various theories. (a) classical nucleation theory (above dashed line) and the Tolman-corrected theory with a constant Tolman length of 0.4 Å. (below dashed line). (b) Tolman-corrected theory with the temperature-dependent Tolman length of Fig. 8.

rates is higher than expected, exceeding an order of magnitude for several Wölk and Strey isotherms. The Wölk and Strey scaled rates also show a systematic positive deviation from our 2003 rates, at equal temperature. This seems to contradict the agreement found earlier in Fig. 5, but the difference is actually caused by the incorrect supersaturation dependence of the CNT nucleation rate, as we will show later.

E. Critical cluster sizes

To determine the critical size with the nucleation theorem of Eq. (7), the slope of the isotherms must be determined. In most cases the isotherms are slightly curved, but when a straight line is fitted to the isotherm, the slope of the line is found to be a good approximation of the slope at the center of the isotherm.

In the case of isotherms that have much scatter or consist of a small number of points, another consideration should be made. The scaled error in $\ln S$ (the error in $\ln S$ times the slope of the line) is higher than the error in $\ln J$, so we fitted the lines by applying the least-squares method in the $\ln S$ direction. That is, in the $\ln J$-$\ln S$ plot of Fig. 5, we minimized the sum of squared *horizontal* residuals. The resulting lines are also shown in that figure. In the case of the isotherms of Wölk and Strey that have little scatter it is not necessary to specify the direction of minimization, because it has only a small (2%) influence on the slope. (Only for the

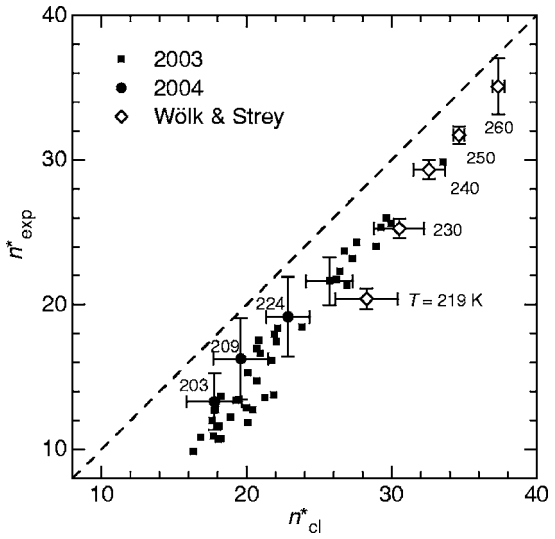

FIG. 7. Experimental critical size found with the nucleation theorem of Eq. (7) as a function of the theoretical critical size of Eq. (5). All experimental points lie below the dashed line of slope unity that indicates perfect agreement. The vertical error bars indicate the 90% confidence intervals representing the random error of fitting in the $\ln J - \ln S$ plot. The horizontal error bars indicate the effect of possible systematic errors in the physical properties; these errors increase with decreasing temperature.

260-K isotherm, which has more scatter, the difference is 9%.)

For comparison with theory we want to assign a single theoretical n^* value to the isotherm, which is not straightforward since n^*_{cl} varies along the isotherm. One could evaluate n^*_{cl} at each isotherm point and then take the mean, as Wölk and Strey did, but we will specify a single reference temperature and supersaturation at which n^*_{cl} is evaluated. It is reasonable to take as a reference supersaturation value the mean of $\ln S$ of the points, because the lines are fitted in a plot with $\ln S$ as abscissa, and fitting a straight line to a curved isotherm gives the slope in the center of this isotherm. As a reference temperature we will take the mean of the temperatures of the isotherm points.

The empirical fit of the 2003 data of Eq. (25) also allows us to obtain an estimate of the critical cluster size. In particular, from Eqs. (7) and (25) we derive that

$$n^*_{\mathrm{fit}} = \left(\frac{\partial \ln J_{\mathrm{fit}}}{\partial \ln S}\right)_T - 1 = \frac{2(b_0 + b_1 T)}{(\ln S)^3}. \tag{28}$$

Using the experimental temperature and supersaturation values, an n^*_{fit} value can be calculated for each experiment of the 2003 series.

In Fig. 7, the experimental critical sizes n^*_{exp}, obtained with the nucleation theorem, are plotted as a function of the theoretical critical sizes n^*_{cl} from Eq. (5). In all cases the experimental value lies below the CNT prediction. The vertical error bars shown are 90% confidence intervals. Our n^*_{exp} values have larger vertical error bars than Wölk and Strey's because our isotherms have more scatter and consist of fewer experimental points.

Contrary to our findings, Wölk and Strey[3] concluded that their experimental critical sizes did agree with the n^*_{cl} predictions. There are three reasons for this difference. First, we fitted lines to the isotherms by minimizing horizontal—instead of vertical—residuals in the $\ln J$-$\ln S$ plot. Second, Wölk and Strey used the nucleation theorem in the form $n^* = (\partial \ln J / \partial \ln S)$, ignoring the supersaturation dependence of the kinetic prefactor K. Our expression has $(\partial \ln J / \partial \ln S) - 1$ at the right-hand side, so that we find n^*_{exp} values that are 1 lower than theirs. The largest difference is caused by our model for the surface tension, which gives up to 4.5% higher values than the Wölk and Strey fit (see Appendix). As a result, our n^*_{cl} values are higher than those found by Wölk and Strey.

In Sec. V F we describe how the differences between n^*_{exp} and n^*_{cl} can be explained in the framework of Tolman's theory.

F. Estimation of the Tolman length

In the earlier description of the Tolman correction, clusters were measured by their radius, whereas the experimental critical sizes are found as numbers of molecules. With the help of the equimolar dividing surface from Eq. (10), the radius can be related to the number of molecules,

$$\tfrac{4}{3}\pi (R^*_e)^3 = n^* v_1 \quad \text{or} \quad R^*_e = R_1 (n^*)^{1/3}, \tag{29}$$

with $R_1 = (3v_1/4\pi)^{1/3}$. From Eq. (16) it then follows that the real critical cluster size differs from the classical size as

$$n^* = [(n^*_{\mathrm{cl}})^{1/3} - \delta/R_1]^3, \tag{30}$$

where we also used that $R^*_{\mathrm{cl}} = R_1 (n^*_{\mathrm{cl}})^{1/3}$. Rewriting Eq. (30) gives the Tolman length as a function of the real and classical critical sizes,

$$\delta = R_1 [(n^*_{\mathrm{cl}})^{1/3} - (n^*_{\mathrm{exp}})^{1/3}], \tag{31}$$

where we wrote the real critical size as n^*_{exp} to indicate that this is the quantity that is found from experiments. Equation (31) can be used to calculate the Tolman length from a plot such as Fig. 7, where a δ value is found for each $(n^*_{\mathrm{cl}}, n^*_{\mathrm{exp}})$ point. The resulting δ values are plotted in Fig. 8 as a function of the nucleation temperature. All Tolman lengths are positive because, as we saw earlier, the experimental critical sizes are smaller than predicted. The δ values that belong to our 2003 results agree well with the δ calculated from the Wölk and Strey data and suggest that δ increases with decreasing temperature, reaching a value of about 0.9 Å at 200 K. The δ's from the 2004 results, on the other hand, do not exhibit such a strong temperature dependence and lie lower than the other two datasets. The error bars are rather large, so the 2004 δ's cannot be said to disagree with the other results.

Now that we know the size and magnitude of the Tolman length, we will examine how it influences the nucleation rate predictions. We start by analyzing the effect of a constant δ of 0.4 Å, arbitrarily chosen as an average value in the range of 200–260 K. The corrected nucleation rate J_{Tol} of Eq. (19) then predicts a nucleation rate that is about six orders of magnitude higher than the J_{cl} rate. This is illustrated by the $J_{\mathrm{exp}}/J_{\mathrm{Tol}}$ ratio in Fig. 6(a) that is consequently about six orders lower. Apart from this vertical offset, the vertical scatter in our data as well as the data of Wölk and Strey decreases

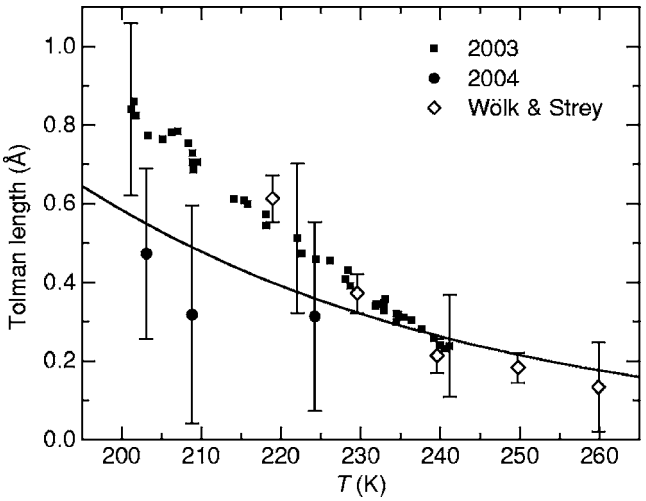

FIG. 8. Temperature dependence of the Tolman length, calculated from the difference between theoretical and experimental critical sizes, [Eq. (31)]. The error bars indicate the 90% confidence intervals, excluding the influence of systematic errors in physical properties. Typical errors of the points of the 2003 series are shown on three points. The line shows a possible exponential temperature dependence of the Tolman length that improves the temperature dependence of the theoretical nucleation rate [see Fig. 6(b)].

(note the scatter of the 219-K Wölk and Strey isotherm, which is almost halved). Of course, this reduction of scatter is a result of the improved supersaturation dependence of the theoretical rate J_{Tol}. Another result is the agreement between our 2003 results and those of Wölk and Strey in the range of 220–240 K, confirming the agreement of the absolute rates already found in Fig. 5.

Let us now see how a temperature-dependent Tolman length influences the predictions. As an example, we take an exponential dependence, $\delta(T)=0.32\ \exp[-(T-230)/50]$ with T in K and δ in ångström. This form of $\delta(T)$ makes the temperature dependence of the corrected theoretical rate J_{Tol} agree with experiments, as can be seen in Fig. 6(b) where the $J_{\mathrm{exp}}/J_{\mathrm{Tol}}$ ratio does not depend on temperature. In fact, this $\delta(T)$ was chosen to have exactly this effect on the theoretical rate; it should not be regarded as an experimental measurement or as a "best fit" to the Tolman lengths of Fig. 8. Aside from that, we see from Fig. 6(b) that a division of the corrected rate J_{Tol} by a factor of 100 would bring the rates in agreement with both the 2003 results and those of Wölk and Strey, within one order of magnitude.

VI. CONCLUSION AND DISCUSSION

We have presented new homogeneous nucleation rate measurements of water in helium in the range of 200–240 K. In the temperature range where a comparison with the Wölk and Strey results is possible (220–240 K) a good agreement of nucleation rates is found (within half an order of magnitude); the supersaturation dependence also agrees. The supersaturation dependence of both our rates and those of Wölk and Strey is lower than classical theory predicts, which means that the number of of molecules in a critical cluster is also smaller than the CNT value.

Including Tolman's size-dependent surface tension gives a different prediction of the critical size, in which one free parameter remains: the Tolman length, describing the strength of the size dependence of surface tension. By matching the experimental critical sizes with the Tolman predictions, the Tolman length could be determined. We find a positive Tolman length, which means that the surface tension decreases with decreasing droplet size. The magnitude of the Tolman length increases with decreasing temperature, from about 0.1 Å at 260 K to (0.6 ± 0.4) Å at 200 K. These values are of the same order as the molecular diameter of water, which is commonly used as an estimate of the Tolman length.[14,30] Abraham[17] estimated δ at half the thickness of a molecular layer in the liquid and gave for water a value of $\delta\approx 1$ Å, which is comparable to our findings.

We developed a nucleation rate expression that includes the Tolman size-dependent surface tension. For a constant positive Tolman length of 0.4 Å, the corrected rates have an improved supersaturation dependence and are about 10^6 times higher than the CNT rates. As an illustration, we have shown that including a temperature-dependent Tolman length may also bring the temperature dependence of the rates in agreement with experiment. Then only a division by a constant factor is needed to make the theoretical rates agree within one order of magnitude with our experiments of 2003 and those of Wölk and Strey.

The nucleation rates of our 203-K isotherm of the 2004 series deviate about one order of magnitude from the 2003 rates, as can be seen in Fig. 5. This systematic deviation cannot be explained by the experimental uncertainty of the nucleation rates; therefore, it can be said that the 2003 and 2004 rates do not agree with each other at low temperature. Moreover, the slope of the 203-K isotherm also deviates from the slope of the 2003 fit, which results in lower Tolman lengths of the 2004 data. We have tried to find a reason for the differences; possibly, the 2004 results were influenced by a change in measurement position (in 2004, the distance between the laser beam and the end wall was increased from 5 to 25 mm). However, according to numerical simulations,[31] this change should not influence the nucleation conditions. The issue is therefore still unresolved.

The values we obtained for the Tolman length should be regarded as rough estimates. In deriving Eq. (A2) it was assumed that δ/R is small, which is not the case for all experiments. For example, the experiment with the smallest n^* of 10 has a δ of about 0.8 Å giving $\delta/R_e^*\approx 0.2$, so that $\delta\ll R$ is no longer satisfied. Moreover, the predictions of the Tolman length are sensitive to the surface-tension model that is used, because σ_∞ appears as a third power in the n_{cl}^* formula of Eq. (5). If an alternative surface-tension model is used (the IAPWS model of the Appendix) we find that the low-temperature (200–210 K) Tolman lengths decrease by about 0.25 Å. Still, we may conclude that the Tolman length is positive and significantly differs from zero in the range 200–250 K. Therefore, to accurately predict the supersaturation dependence of the nucleation rate of water, classical nucleation theory cannot be used without modification.

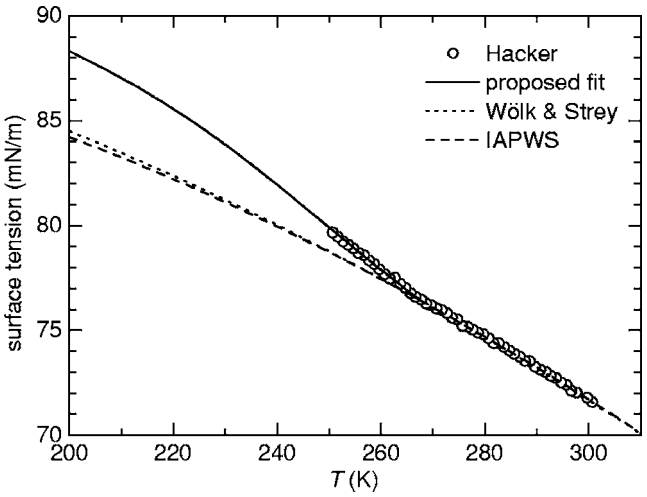

FIG. 9. Surface tension of liquid water and its extrapolation down to 200 K. Both the IAPWS fit (Ref. 35) of Eq. (A1) and the fit of Wölk and Strey (Ref. 3) agree with Hacker's data (Ref. 33) for temperatures higher than about 268 K. The proposed fit of Eq. (A2) reproduces the slope of Hacker's low-temperature data, in contrast to the other fits.

ACKNOWLEDGMENT

We thank Dr. J. Hrubý for his encouragement and for his most valuable contribution to the estimates of the low-temperature thermophysical properties of water.

APPENDIX: THERMOPHYSICAL PROPERTIES OF WATER

Expressions for the density and equilibrium vapor pressure of water were taken from Wölk and Strey.[3] The uncertainty of the density was estimated at 0.1% at 260 K and 2% at 200 K, that of the vapor pressure at 0.2% at 260 K and 1% at 200 K. For the molar mass we used the value $M = 18.015\,268$ g/mol.[32]

For the surface tension, we developed a new fit based on Hacker's accurate measurements[33] down to 251 K (shown in Fig. 9), a model of supercooled water,[34] and the IAPWS equation[35,36]

$$\sigma_{\mathrm{ref}}(T) = B\tau^{\mu}(1 + b\tau) \quad \text{with} \quad \tau = 1 - T/T_c. \tag{A1}$$

The values of B, μ, b, and T_c were taken from Ref. 35 and are listed in Table I. As Fig. 9 shows, the IAPWS expression differs little from the polynomial equation used by Wölk and Strey.[3] IAPWS endorses the validity of Eq. (A1) between 273 K and the critical point; a comparison with the Hacker data in Fig. 9 shows that the validity range can be extended down to about 268 K. For lower temperatures we propose the fit

$$\sigma(T) = \sigma_{\mathrm{ref}}(T) - \sigma_a \tanh[(T - T_a)/T_b] + \sigma_b \quad (T < 267.5\ \mathrm{K}), \tag{A2}$$

where σ_a, σ_b, T_a, and T_b are shown in Table I. This fit agrees with the Hacker data to within 0.2% and may be extrapolated down to 100 K. At 200 K the estimated uncertainty is 2.5%.

TABLE I. Parameters used in the surface tension fits, Eqs. (A1) and (A2).

Parameter	Value	Parameter	Value
B(N/m)	0.2358	σ_a(N/m)	2.854×10^{-3}
T_c(K)	647.096	σ_b(N/m)	1.666×10^{-3}
μ	1.256	T_a(K)	243.9
b	−0.625	T_b(K)	35.35

[1] C. T. R. Wilson, Philos. Trans. R. Soc. London, Ser. A **189**, 265 (1897).
[2] J. Wölk, R. Strey, C. H. Heath, and B. E. Wyslouzil, J. Chem. Phys. **117**, 4954 (2002).
[3] J. Wölk and R. Strey, J. Phys. Chem. B **105**, 11683 (2001).
[4] P. Peeters, J. J. H. Gielis, and M. E. H. van Dongen, J. Chem. Phys. **117**, 5647 (2002).
[5] D. G. Labetski, V. Holten, and M. E. H. van Dongen, J. Chem. Phys. **120**, 6314 (2004).
[6] R. Becker and W. Döring, Ann. Phys. **24**, 719 (1935).
[7] H. Reiss, W. K. Kegel, and J. L. Katz, J. Phys. Chem. A **102**, 8548 (1998).
[8] D. Kashchiev, J. Chem. Phys. **118**, 1837 (2003).
[9] V. I. Kalikmanov, J. Chem. Phys. **121**, 8916 (2004).
[10] D. Reguera and H. Reiss, J. Phys. Chem. B **108**, 19831 (2004).
[11] G. Wilemski, J. Chem. Phys. **103**, 1119 (1995).
[12] C. L. Weakliem and H. Reiss, J. Phys. Chem. **98**, 6408 (1994).
[13] D. Kashchiev, J. Chem. Phys. **76**, 5098 (1982).
[14] D. Kashchiev, *Nucleation: Basic Theory with Applications* (Butterworth-Heinemann, Oxford, 2000).
[15] R. K. Bowles, D. Reguera, Y. Djikaev, and H. Reiss, J. Chem. Phys. **115**, 1853 (2001).
[16] R. C. Tolman, J. Chem. Phys. **17**, 333 (1949).
[17] F. F. Abraham, *Homogeneous Nucleation Theory* (Academic, New York, 1974).
[18] J. W. P. Schmelzer and V. G. Baidakov, J. Chem. Phys. **119**, 10759 (2003).
[19] K. N. H. Looijmans, P. C. Kriesels, and M. E. H. van Dongen, Exp. Fluids **15**, 61 (1993).
[20] K. N. H. Looijmans and M. E. H. van Dongen, Exp. Fluids **23**, 54 (1997).
[21] P. Peeters, J. Hrubý, and M. E. H. van Dongen, J. Phys. Chem. B **105**, 11763 (2001).
[22] Y. Viisanen, R. Strey, and H. Reiss, J. Chem. Phys. **99**, 4680 (1993).
[23] R. C. Miller, R. J. Anderson, J. L. Kassner, and D. E. Hagen, J. Chem. Phys. **78**, 3204 (1983).
[24] J. L. Schmitt, J. Whitten, G. W. Adams, and R. A. Zalabsky, J. Chem. Phys. **92**, 3693 (1990).
[25] G. J. Doster, J. L. Schmitt, and G. L. Bertrand, J. Chem. Phys. **113**, 7197 (2000).
[26] J. Wölk, Ph.D. thesis, Universität zu Köln, 2001.
[27] C. C. M. Luijten and M. E. H. van Dongen, J. Chem. Phys. **111**, 8524 (1999).
[28] C.-H. Hung, M. J. Krasnopoler, and J. L. Katz, J. Chem. Phys. **90**, 1856 (1989).
[29] R. Strey, P. E. Wagner, and T. Schmeling, J. Chem. Phys. **84**, 2325 (1986).
[30] V. I. Kalikmanov, Phys. Rev. E **55**, 3068 (1997).
[31] X. Luo, Ph.D. thesis, Eindhoven University of Technology, 2004.
[32] W. Wagner and A. Pruß, J. Phys. Chem. Ref. Data **31**, 387 (2002).
[33] P. T. Hacker, Technical Note 2510, National Advisory Committee for Aeronautics (1951), URL http://naca.larc.nasa.gov/reports/1951/naca-tn-2510/
[34] J. Hrubý, in *Nucleation and Atmospheric Aerosols 2004*, edited by M. Kasahara and M. Kulmala (Kyoto University Press, Kyoto, 2004), p. 135.
[35] *IAPWS Release on Surface Tension of Ordinary Water Substance*, IAPWS (1994), URL http://www.iapws.org/relguide/surf.pdf, also available from the IAPWS Executive Secretary, Dr. R. B. Dooley, Electric Power Research Institute, 3412 Hillview Av., Palo Alto, CA 94304, USA.
[36] N. B. Vargaftik, B. N. Volkov, and L. D. Voljak, J. Phys. Chem. Ref. Data **12**, 817 (1983).